*Int. J. Electrochem. Sci.*, 15 **(2020)** 3922 – 3934, doi: 10.20964/2020.05.78

International Journal of
ELECTROCHEMICAL
SCIENCE
www.electrochemsci.org

# Reduced Graphene/Polydopamine-Supported Au@Pt/Au Nanoparticles for Electrochemical Detection of Acetaminophen

*Ling Shi*[1,2], *Zefeng Wang*[1,2,*], *Na Wu*[1,2], *Xianlan Chen*[1,2], *Guangming Yang*[1,2,*], *Wei Liu*[1,2,*]

[1] School of science, Honghe University, mengzi, Yunnan 661199, PR China
[2] Key Laboratory of Natural Pharmaceutical & Chemical Biology of Yunnan Province, Mengzi, Yunnan 661199, PR China
[*]E-mail: wangzefeng841006@163.com, yangguangmingbs@126.com, liuwei4728@126.com

*Received:* 13 January 2020 / *Accepted:* 8 March 2020 / *Published:* 10 April 2020

In this work, we report an efficient electrochemical sensor made from reduced graphene/polydopamine supported Au@Pt/Au (GN/PDA/Au@Pt/Au) nanoparticles for detection of acetaminophen (ACOP). The electrochemical reaction mechanism is investigated using cyclic voltammetry (CV). The Electrocatalytic activity is monitored under varying pH. The ACOP is detected under the optimal condition. A linear range from 1 to 300 μM is achieved with a limit of detection of 0.31 μM. The fabricated sensor show satisfactory results in commercial tablets.

**Keywords:** graphene; polydopamine; Au; Pt; electrochemical sensor; acetaminophen

## 1. INTRODUCTION

Acetaminophen (ACOP) is an important pharmaceutical analgesic and antipyretic drug. It is widely applied to relief moderate pain associated with backache, headache, arthritis, and postoperative pain. It is also used as antipyretic drug and widely used to cure influenza disease [1, 2]. However, the overdoses of ACOP can cause the accumulation of toxic metabolites, and can cause severe kidney and liver damage [3, 4]. Thus, it is crucial important to develop facile and accurate analytical method for the determination of ACOP in medical and pharmaceutical fields. At present, a variety of analytical technologies have been used to detect the ACOP. For example, high-performance liquid chromatography [5], fluorescence spectroscopy [6], chemililuminescence [7], capillary electrophoresis [8], and so on. Nevertheless, these analysis technologies usually have complex pretreatment procedures, intricate operate process, long-time detection, and expensive apparatuses. The electrochemical analysis technology has attracted much attention due to instrument simplicity, easyto-operate, low cost, fast response and excellent sensitivity [9, 10].

Graphene (GN) possesses exceptional thermal and conductivity properties, large specific surface area [11], which has been widely used in sensor [12], supercapacitors [13], hydrogen storage [14], and so on, especially in electrochemical sensor field. However, the pure GN has poor water solubility and limits its application. To exploit the potential application, one promising strategy is use GN as substrate to anchor nanomaterials. Bioactive materials as the surface coating functional materials are usually used to improve the performance of GN. Polydopamine (PDA) has received large attention due to its excellent biocompatible and conductive, which has been used as functional materials. PDA is liable to coat on the surface of GN and can be a good support for nanoparticles [15, 16]. On the other hand, bimetallic nanoparticles (NPs) with alloyed nanostructures usually possess outstanding properties compared with the monometallic [17, 18]. The composition of alloy has an enormous impact on the properties of obtained alloy. Recently, the combination of Pt and Au NPs offers an attractive technological application. For example, methanol fuel [19], electrochemical sensors [20], catalysts [21], and so on.

In the present work, we design a simple method to synthesize GN/PDA-Au@Pt/Au nanoflowers, and a novel electrochemical sensor based on GN/PDA-Au@Pt/Au nanoflowers. PDA can be easily polymerized onto the surface of GN to form GN/PDA nanocomposites. Meantime, the obtained GN/PDA nanocomposites can be used as substrate to anchor Pt and Au alloy NPs. The obtained GN/PDA-Au@Pt/Au nanoflowers coated glass carbon electrode (GN/PDA-Au@Pt/Au/GCE) is developed as electrochemical sensor for ACOP detection. The fabricated sensor reveals good selectivity and stability for detection of ACOP.

## 2. EXPERIMENTAL

### *2.1 Reagents*

Graphite (99.95%, 8000 mesh) powder and dopamine hydrochloride (98%) are obtained from Alfa Aesar. $HAuCl_4$ (99.99%, wt.%) and $H_2PtCl_6$ (≥99.8, wt.%) are obtained from Shanghai Sybridge Chemical reagent Company. Trisodium citrate, acetaminophen and other reagents are obtained from Shanghai Chemical Reagent Co. Ltd. (Shanghai, China). Britton-Robinson (B-R) buffer solutions (0.04 M in each of acetic, phosphoric and boric acids) adjust to the desired pH with additions of 0.2 M sodium hydroxide are used as a supporting electrolyte. Ultra-pure water is obtained with a Milli-Q plus water purification system (Millipore Co. Ltd., USA) (18 M).

### *2.2 Apparatus*

UV-vis absorption spectra are performed at the UV-vis spectra (Perkin-Elmer Lambda 900 USA).The the sizes and morphology of the obtained nanomaterials are characterized with transmission electron microscope (TEM, JEM-2100, JEOL, Japan). X-ray diffraction (XRD, X'Pert$^3$ powder diffractometer, PANAlytical Company) is used to characterize crystal structures and phase composition of as-prepared nanomaterials. X-ray photoelectron spectroscopy (XPS) experiments are performed on

a *K-Alpha*$^+$ spectrometer (Thermo fisher Scientific) with Al Kα radiation (hν = 1486.6 eV). Electrochemical testings are performed on CHI 660E electrochemical workstation (CHI, Shanghai). A standard three electrode system, consisting of a nanomaterials-modified glass carbon electrode (GCE, 3mm diameter) as working electrode with a platinum wire counter electrode and Ag/AgCl electrode reference electrode are used throughout the experiment.

### *2.3 Synthesis of Au nanoseeds*

Au nanoseeds are synthesized according to a modified Frens' method [22]. 1.296 mL 19.302 mM $HAuCl_4$ solution is added into 48.8 mL ultra-pure water in a flask. Then the obtained solution is heated to a boil. Subsequently, 0.368 mL 340 mM trisodium citrate solutions are added into the above mixture solution. The mixtures are vigorous stirred and refluxed for 10 min. Finally, the obtained wine red dispersion is stored at 4℃ after cooling.

### *2.4 Preparation of GN/PDA nanocomposites*

Graphite oxide (GO) is prepared from graphite flake according to a modified Hummers's method [23]. The GN/PDA nanocomposites are prepared according to the following method. The GO (60 mg) is dispersed in ultra-pure water (80 mL) and ultrasound for 2 h. Then, dopamine hydrochloride (40 mg) is added into the GO suspension. After vigorous sonication for 30 min at room temperature, 40 mL of 12.5 mM Tris-HCl solution (pH = 8.5) is added. The obtained mixture is stirred at 80 ℃ for 24 h. Finally, the obtained products are centrifuged and washed with ultrapure water and then dispersed in ultrapure water.

### *2.5 Preparation of GN/PDA-Au@Pt/Au nanoflower*

The GN/PDA (10 mg) is mixed with Au seeds (14.3 mL, 1.4 mg/mL) and sonication for 4 h. $HAuCl_4$ (10 mg) and $H_2PtCl_4$ (10 mg) are added into above mixture solution. Subsequently, trisodium citrate solution (14.705 mg) is added into the above solution. The whole solution is 20 mL. The obtained mixture solutions are vigorously sonication for 30 min at ice-bath. Then fresh ice-cold $NaBH_4$ solution (1.2 mL, 0.1 M) is added into the above solution at stirring for 30 min. Finally, the obtained products are centrifuged and washed with ultrapure water and then dispersed in ultrapure water.

### *2.6 Preparation of electrode and analytical procedure*

The bare GCE is thoroughly polished with $Al_2O_3$ (1.0, 0.3 and 0.05 μm), then sonicated successively in 1:1 nitric acid solution, ethanol and ultrapure water, and then dried with nitrogen gas. Then 7 μL 1 mg/mL of as-prepared GN/PDA-Au@Pt/Au nanoflower suspension is dropped onto GCE and dried in air, respectively. CV and DPV experiments are carried out in B-R buffer solutions containing a constant concentration of ACOP.

## 3. RESULT AND DISCUSSION

### *3.1 Characterization of prepared nanomaterials*

Figure 1 shows the UV-vis absorption spectra of prepared nanomaterials. The Au nanoparticles (NPs) reveals a dominant signal peak at 520 nm, which is designated as the dipole mode of surface plasmon resonance of Au NPs [24]. GN displays a strong absorption peak around 262 nm, which is designated to π-π* transitions of the aromatic C=C band (cure b). When PDA is modified onto the surface of GN, the absorption peak is wider than the pure GN (cure c), which displays that the GN has been successfully functionalized. As for the GN/PDA-Au@Pt/Au nanoflowers, there are two obvious absorption peak can be observed. The absorption peak at about 520 nm is obviously wider than the pure Au NPs which is due to the interaction between GN, Pt and Au.

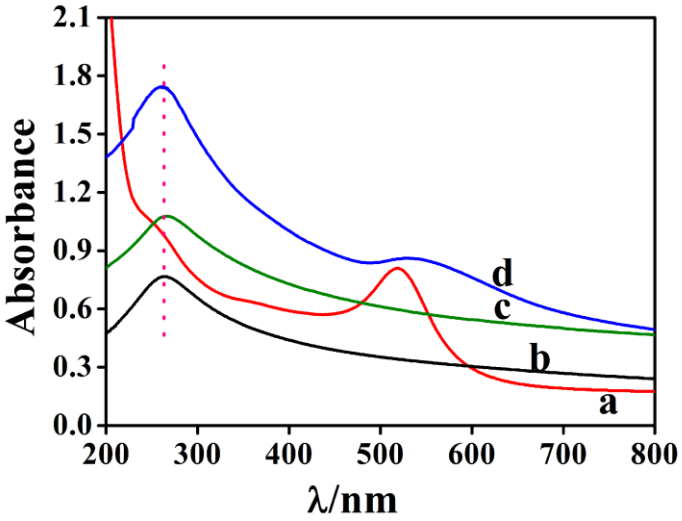


**Figure 1.** UV-vis spectra of (a) Au, (b) GN, (c) GN/PDA, and (d) GN/PDA-Au@Pt/Au nanoflowers.

The prepared GN/PDA-Au@Pt/Au nanoflower is further analyzed by XPS. The survey scan spectrum of GN/PDA-Au@Pt/Au nanoflower (Figure 2a) displays that the obtained nanoflowers are contained C, N, O, Au and Pt elements. The spectrum of C1s can be deconvoluted into three peaks at 284.8, 286.3 eV, and 288.5 eV, which can be attributed to the C-C, C-OH and C=O bonds (Figure 2b), respectively [10]. The peaks at 400.3 eV in the N1s spectrum (Figure 2c) are attributable to -N= bond of the PDA [25]. The spectrum of O1s can be deconvoluted into two species centered at 531.4 and 533.0 eV, which corresponds to the C=O and C-O bands, respectively (Figure 2D). Figure 2E shows the high-resolution spectra of Pt 4f, the Peaks at 71.6 eV and 75.0 eV originated from Pt $4f_{7/2}$and Pt $4f_{5/2}$, respectively [26]. The peaks located at about 84.2 eV and 87.9 eV can be contributed to Au $4f_{7/2}$and Au $4f_{5/2}$, respectively (Fig. 6C) [27].

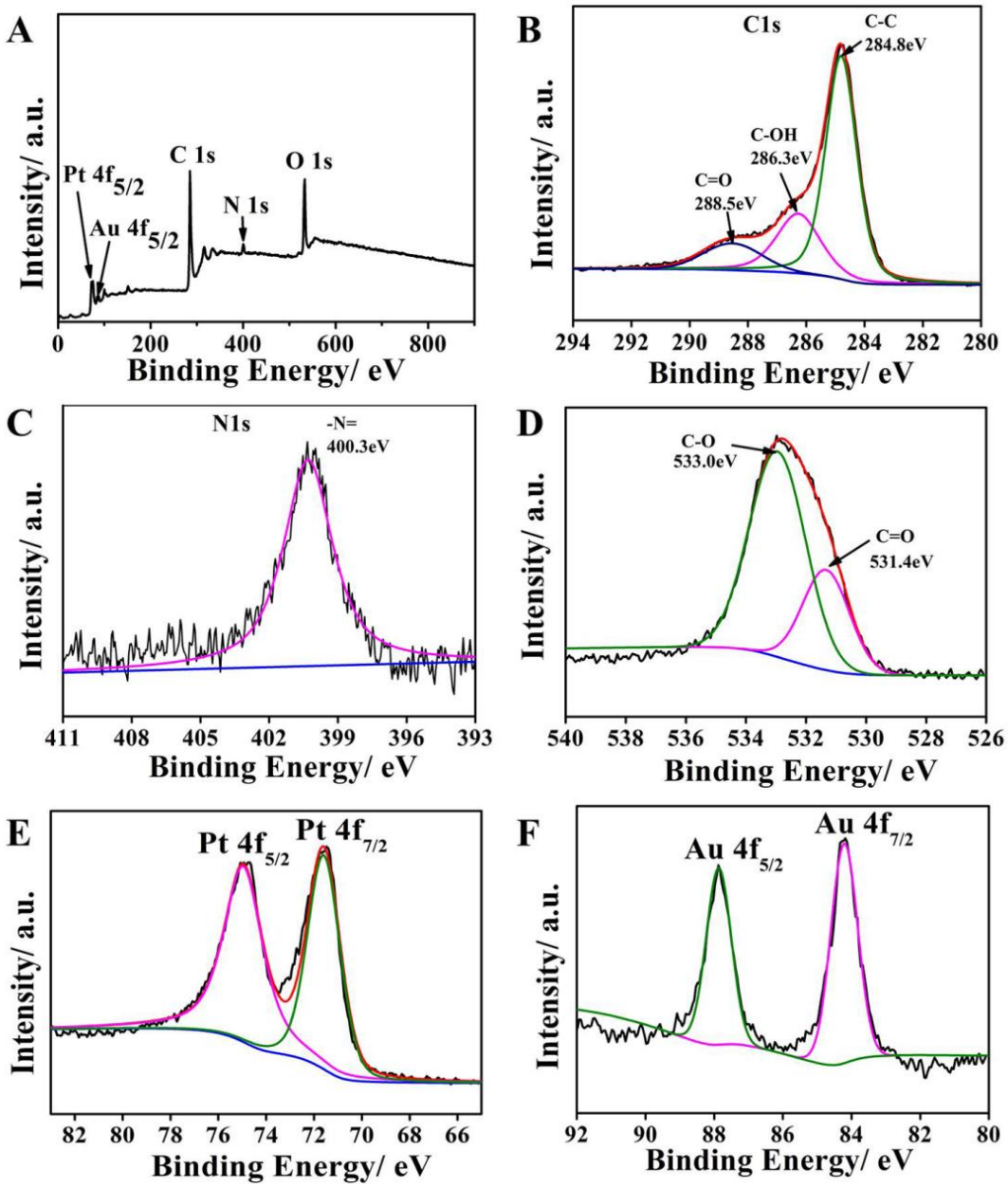


**Figure 2.** Survey of GN/PDA-Au@Pt/Au nanoflowers (A), and high-resolution (B) C1s, (C) N1s, (D) O1s, (E) Pt4f and (D) Au4f spectra of GN/PDA-Au@Pt/Au nanoflowers.

The morphological of the prepared nanoflowers is characterized by TEM and HRTEM images. Figure 3A shows the TEM image of GN/PDA-Au@Pt/Au nanoflowers, the flower-like Au@Pt/Au is monodispersed on GN/PDA, and only some alloy nanoparticles exist in the form of small clusters. The GN/PDA shows a transparent film structure. From HRTEM images, the size of the nanoflowers is about 35 nm can be observed.

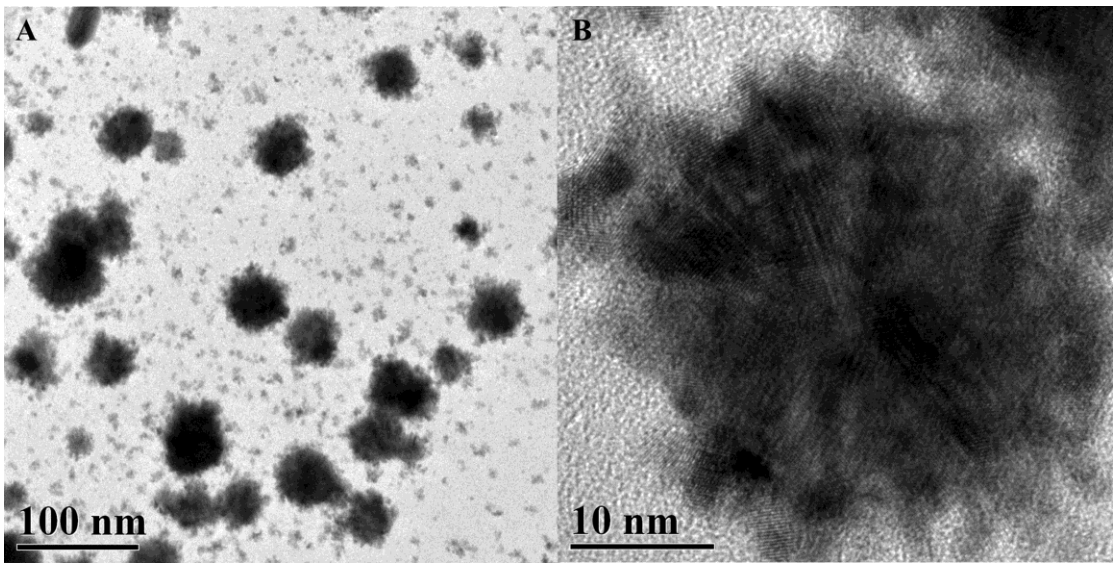


**Figure 3.** TEM (A) and HRTEM (B) images of GN/PDA-Au@Pt/Au nanoflowers.

XRD analysis is carried out to detect the internal lattice of prepared nanomaterials. Figure 4 shows the XRD patterns of GN, GN/PDA and GN/PDA-Au@Pt/Au. GN shows a broad diffraction peak centered at 22.0° (curve a), which is in agreement with the literature reported [28, 29]. Curve b shows the XRD patters of GN/PDA, a very broad diffraction peak appears at 2θ=24.1° can be observed. This result proves that the PDA has successfully doped into the GN. Figure 4c shows the XRD patterns of GN/PDA-Au@Pt/Au, the diffraction peaks at 38.2°, 44.5°, 64.8°, 77.8°, and 82.0° are corresponded to the (111), (200), (220), (311), and (222) facets, respectively. These diffraction peaks are in accordance with the diffraction standard of Au (JCDPF-04-0784) [30] and Pt (JCPDF 04-0802) [31], which shows face-centered-cubic (fcc) structure of Au and Pt.

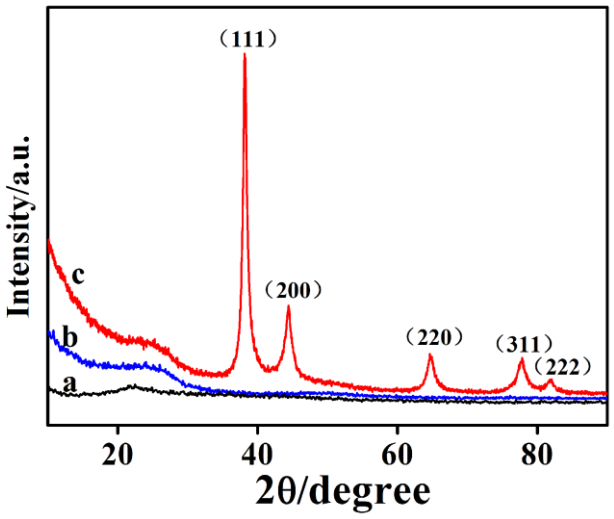


**Figure 4.** XRD patterns of (A) GN, (B) GN/PDA and (C) GN/PDA-Au@Pt/Au nanoflowers.

*3.2 Electrochemical behaviors of ACOP*

Figure 5 shows CVs of bare GCE (curve a), Au/GCE (curve b), and GN/PDA-Au@Pt/Au/GCE (curve c) in $N_2$-saturated pH=6.0 B-R buffer solution containing 300 μM ACOP. Bare GCE and Au/GCE show a weak oxidation peaks. And the peak potential separation (△Ep) is very large. However, a pair of well-defined redox peaks is noticed at GN/PDA-Au@Pt/Au/GCE, and the current intensity is larger than the bare GCE and Au/GCE. Meantime, the value of △Ep is obvious littler than bare GCE and Au/GCE. These results imply that the prepared GN/PDA-Au@Pt/Au nanoflower can effectively enhanced electron transfer of ACOP. And further improve that the obtained GN/PDA-Au@Pt/Au nanoflower possesses excellent electrocatalytic activity. That maybe due to the GN has large surface area which is benefit for adsorbing ACOP. Au NPs can offer a large sensing platform for the recognition of ACOP. These excellent performances can be synergistically enhancement.

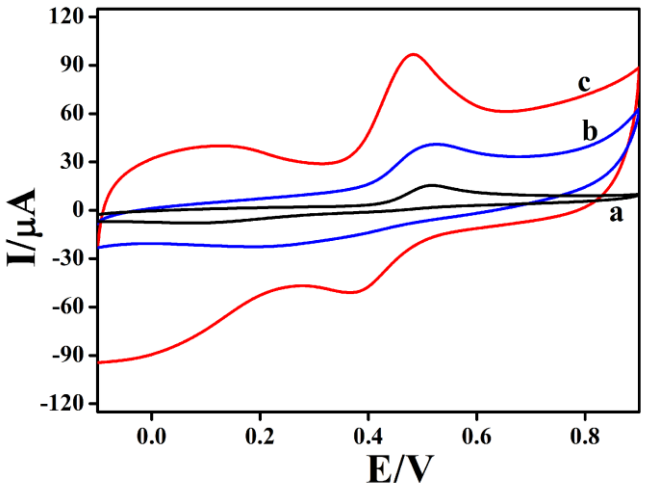


**Figure 5.** CVs of 300 μM ACOP obtained at (a) bare GCE, (b) Au/GCE, and (c) GN/PDA-Au@Pt/Au/GCE in $N_2$-saturated B-R solution (pH 6.0).

The electrooxidation mechanism of the ACOP on fabricated sensor is investigated by CV. Figure 6A shows the CVs observed for the electrochemical oxidation of ACOP at GN/PDA-Au@Pt/Au/GCE for different scan rates (40-600 mV/s). We can see that the redox peak currents are continuously increased with increasing scan rate. Figure 6B reveals that the redox peak currents of ACOP are linearly proportional to scan rate (ν). The linear regression equations as: $I_{pa}$=0.5933ν+37.4281 ($R^2$=0.9945) and $I_{pc}$=-0.3666ν-13.5469 ($R^2$=0.9973). These results indicate that the oxidation of ACOP at GN/PDA-Au@Pt/Au modified electrode is surface-controlled process [32, 33]. Figure 6C reveals that the anode ($E_{pa}$) and cathode ($E_{pc}$) peak potential have good linear relationships with the logarithm of scan rate (lnν). The regression equation is $E_{pa}$=0.0436lnυ+0.2851, $R^2$=0.9892 and $E_{pc}$=-0.0181lnυ-0.4584, $R^2$=0.9297. According to the Laviron equation [34], the electron transfer rate constant ($k_s$), electron transfer number (n), and charge transfer coefficient (α) can be calculated. Here, the slope value from the plot of anodic peak potential ($E_{pa}$) versus lnυ is equal to RT/(1-α)nF and the slope value from the plot of cathode peak potential ($E_{pc}$) versus lnυ is equal to

RT/αnF, respectively.

$$E_{pa} = E^{0'} + \frac{RT}{(1-\alpha)nF}\ln\upsilon \qquad \text{Eq. (A.1)}$$

$$E_{pc} = E^{0'} - \frac{RT}{\alpha nF}\ln\upsilon \qquad \text{Eq. (A.2)}$$

$$\lg k_S = \alpha\lg(1-\alpha) + (1-\alpha)\lg\alpha - \lg\frac{RT}{nF\upsilon} - \alpha(1-\alpha)\frac{nF\Delta E_p}{2.3RT} \qquad \text{Eq. (A.3)}$$

Where $E_p$ is the peak potential, $E^{0'}$ is the formal standard potential, R indicates the universal gas constant (R=8.314 J $mol^{-1}$ $K^{-1}$), T denotes the absolute temperature (T=298 K), F is the Faraday's constant (F=96485 C $mol^{-1}$), υ denotes the scan rate. According to the above equation, the value of n, α and $k_s$ can be calculated is 2, 0.71 and 0.53 $s^{-1}$, respectively. Hence, these results imply that the electrochemical oxidation of ACOP is two electron transfer process.

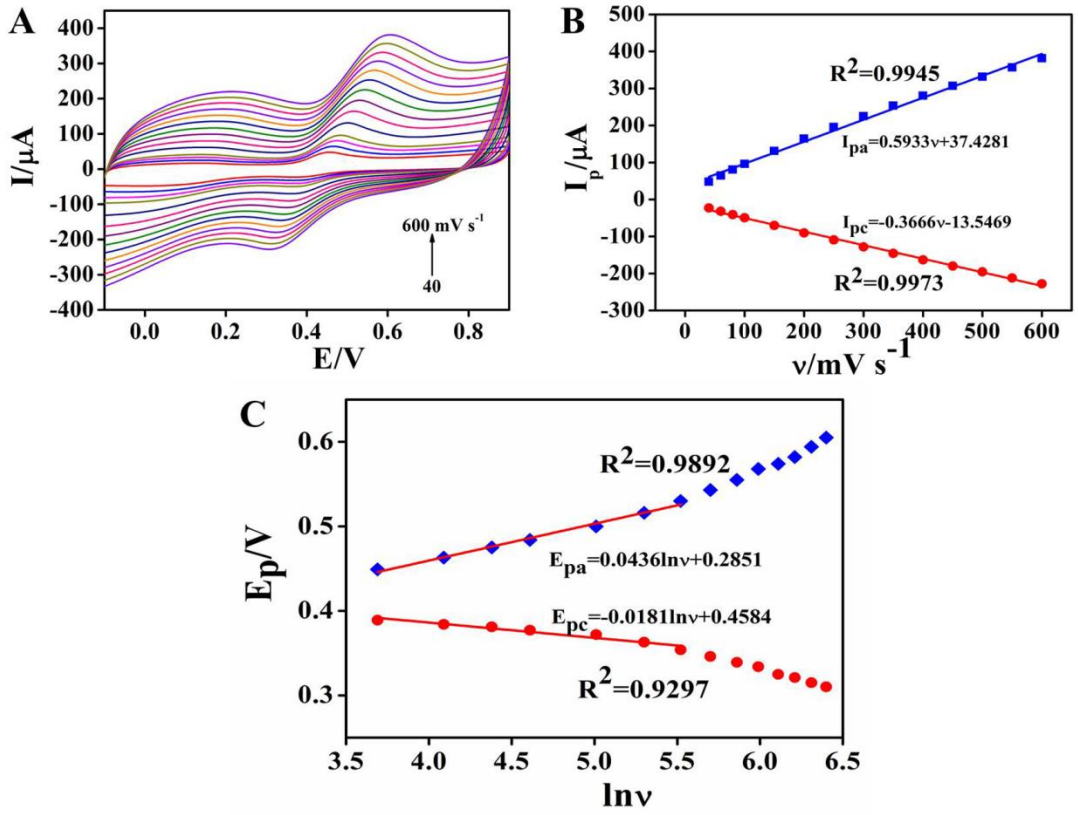


**Figure 6.** (A) CVs of GN/PDA-Au@Pt/Au/GCE in $N_2$-saturated B-R (pH=6.0) buffer solution containing 300 μM ACOP with different scan rates (40 to 600 mV/s). (B) The plots of redox peak current *vs* scan rates. (C) The plots of anodic and cathodic peak potential *vs* lnν.

*3.3 Effect of pH value*

The influence of solution pH on the peak potentials and peak currents of ACOP on the GN/PDA-Au@Pt/Au/GCE are studied with pH value between 3.0 and 8.0 in B-R buffer solution containing 300 μM ACOP. As shown in Figure 7, with the increasing of pH value, the maximum peak current value is obtained at pH=6.0 B-R solution. Thus, pH=6.0 is chosen as supporting electrolyte in

the following experiments. Figure 7B shows a good linearity between peak potential and pH value. The linear equation is: Epa=-0.061pH+0.888 ($R^2$=0.9944), Epc=-0.058pH+0.74 ($R^2$=0.9930), respectively. The slope of the calibration curve -0.061 V and -0.058 V are close to the theoretical value -0.0592 V, revealing that the transferred electron number is equal to the number of protons [34]. Furthermore, based on the formula [35]: dEp/dpH = 2.303mRT/nF, where n is the number of electron, m represents the number of proton. The m/n can be calculated is 1.03 and 0.98 for the oxidation and reduction processes, respectively. It shows that the number of electron and proton in the electrochemical reaction of ACOP is equal [36]. Therefore, the number of electron and proton in electrochemical reaction of ACOP on the GN/PDA-Au@Pt/Au/GCE is almost equal [37]. The oxidation of ACOP at GN/PDA-Au@Pt/Au/GCE can be expressed as the following reaction:

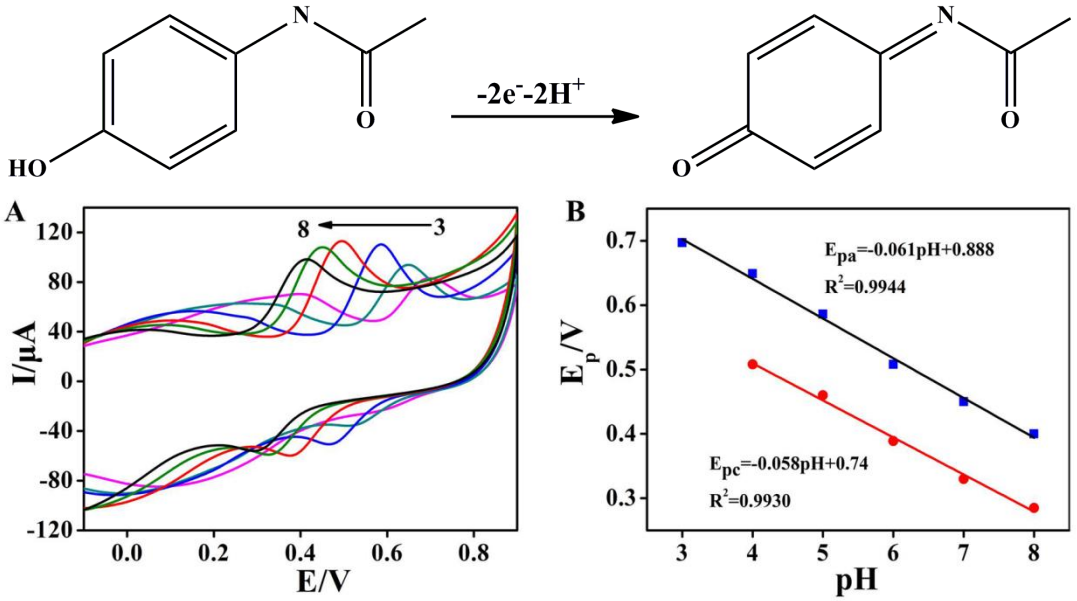


**Figure 7.** (A) CVs obtained of GN/PDA-Au@Pt/Au/GCE in $N_2$-containing B-R buffer solution in different pH values (3.0, 4.0, 5.0, 6.0, 7.0, and 8.0) containing 300 μM ACOP at scan rate of 100 mV/s. (B) The plots of anodic and cathodic peak potential *vs* of pH.

*3.4 detection of ACOP*

The voltammetric sensor of Co-amino-Gr/GCE towards baicalin detection was investigated by Square wave voltammetry (SWV) under optimized conditions. Fig. 9A showed the superimposed SWV curves of baicalin with various concentrations. As shown in Fig. 9B, the anodicstripping currents were linearly increased with baicalin concentrations from 1.0×10−8to 8.0×10−7mol L−1. The linear equation was expressed as ipa(μA)=53.199 C (μM)+1.572 (R=0.999) with a detection limit of 5×10−9mol L−1 (S/N=3). Comparing with other electroanalytical methods reported previously (Table 1), the present method showed a sensitive voltammetric response for determination of baicalin with lower detection limit.

The fabricated GN/PDA-Au@Pt/Au sensor towards ACOP detection is investigated by DPV under the optimal conditions. Figure 8A shows the superimposed DPV curves of ACOP with various concentrations. The peak current is linearly increased with ACOP concentration from 1 to 300 μM. The regression equation is expressed as $I_{pa}$=0.3868C+1.5820 ($R^2$ = 0.9987). The detection limit is 0.31 μM (S/N = 3), which is lower than the one obtained for PTH/MWCNT/CFE (6.0 μM) [38], β-CD/RGO-GCE (2.3 μM) [39], PMG/fCNT/CE (4.3 μM) [40], PEDOT/GO/GCE (0.57 μM) [41]. As shown in Table 1. The results prove that the method exhibits excellent electrochemical activity toward ACOP.

**Table 1.** Comparison of analytical parameters for ACOP determination at different modified electrodes.

| Modified GCE | Linear range/μM | Detection limit/μM | Reference |
|---|---|---|---|
| PTH/MWCNT/CFE | 25-250 | 6.0 | [38] |
| β-CD/RGO-GCE | 10-800 | 2.3 | [39] |
| PMG/fCNT/CE | 25-200 | 4.3 | [40] |
| PEDOT/GO/GCE | 10-60 | 0.57 | [41] |
| GN/PDA-Au@Pt/Au/GCE | 1-300 | 0.31 | This work |

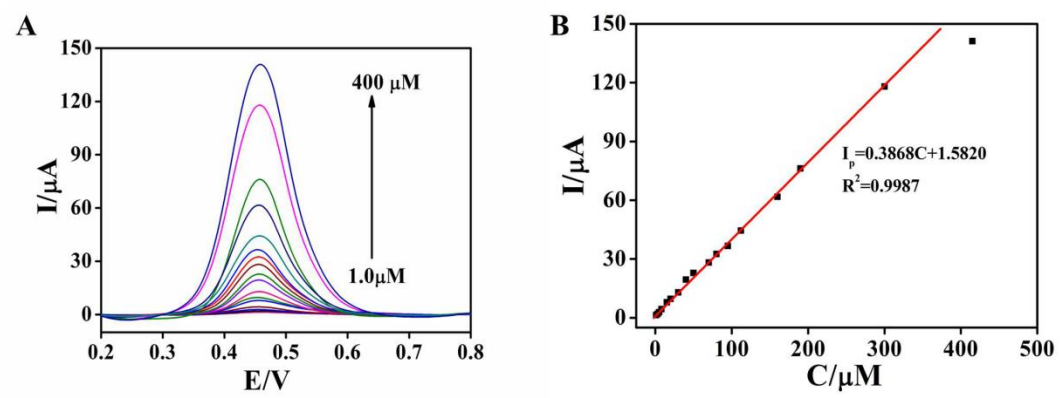


**Figure 8.** (A) DPV curves of GN/PDA-Au@Pt/Au/GCE with different concentrations (1.0-400 μM) ACOP in $N_2$-saturated pH=6.0 B-R buffer solution. (B) The plots of peak current *vs* ACOP concentration.

*3.5 Selectivity, reproducibility, and stability of fabricated sensor*

The selectivity of GN/PDA-Au@Pt/Au/GCE toward ACOP is investigated in the presence of some possible interfering species. The results reveal that only have little response on the detection of 300 μM ACOP.when 2 mM of glucose, ascorbic acid, KCl, NaCl, and $CaCl_2$.Therefore, the fabricated sensor possesses excellent selective for detection of ACOP. The reproducibility of the sensor is also investigated. Five GN/PDA-Au@Pt/Au/GCEs fabricated using the same method are used for the determination of 300 μM ACOP. The results show that the RSD value is 3.1%, which demonstrates the GN/PDA-Au@Pt/Au/GCE have excellent reproducibility. The stability of proposed sensor is also

valuated by CV measurements. The modified GCE is continuously detected for 30 consecutive days. The results show that the current response of sensor is almost no changed. Which confirm that the fabricated sensor has good stability. The results reveal that the fabricated sensor has excellent reproducibility, stability and selectivity.

In order to evaluate the practical application of fabricated sensor, the GN/PDA-Au@Pt/Au/GCE is used to detect the content of ACOP in Compound Paracetamol and Amantadine tablets (0.500 g/tablet). The tablets are purchased from local pharmacy. The tablets are finely powdered in a mortar with pestle and dissolved in ultra-pure water. The solution is filtered and diluted with B-R solution (pH 6.0) for ACOP detection. All the samples are determined in triplicate under the same conditions. The results are shown in Table 2, the content of ACOP in the tablet is calculated to be 248.5 mg/tablet, which is in good agreement with the declared value. In addition, the fabricated sensor also shows an excellent RSD. These results show that the proposed GN/PDA-Au@Pt/Au/GCE sensor is reliable for the determination of ACOP in practical samples.

**Table 2.** Determination of ACOP in Compound Paracetamol and Amantadine tablets.

| sample | Declared (mg/tablet) | Average (mg/tablet) | RSD (%) |
|---|---|---|---|
| 1 | 250 | 247.6 | 2.3 |
| 2 | 250 | 251.3 | 1.1 |
| 3 | 250 | 246.3 | 1.4 |
| 4 | 250 | 248.5 | 2.1 |
| average | 250 | 248.4 | |

## 4. CONCLUSION

In summary, GN/PDA-Au@Pt/Au nanoflower is prepared by an efficient method. The obtained GN/PDA-Au@Pt/Au nanoflower has been characterized by absorption spectra, TEM, XRD, and XPS. The nanoflower obtained is used to fabricated electrochemical sensor for detection of ACOP. The electrochemical reaction mechanism is investigated using cyclic voltammetry (CV). The Electrocatalytic activity is monitored under varying pH. The results show that the prepared nanoflower shows a good electrochemical activity toward ACOP. The ACOP is detected under the optimal condition. A linear range from 1 to 300 μM is achieved with a limit of detection of 0.31 μM. The fabricated sensor show satisfactory results in commercial tablets.

ACKNOWLEDGMENTS
This work supported by the National Natural Science Foundation of China (Grand No. 21665008), the Scientific Research Fund Project of Honghe University (Grand No. XJ14Z02), Junior High School Academic and Reserve Program of Yunnan Province (Grand No. 2018HB005), the Yunnan education department of Scientific Research Foundation (Grand No. 2018JS478), the PhD Start-up Fund of Honghe University (Grand No. XJ16B04), Young Academic Reserve Program of Honghe University (Grand No. 2016HB0401).

**References**


1. F. Li, R. X. Li, Y. Feng, T. Gong, M. Z. Zhang, L. Wang, T. J. Meng, H. X. Jia, H. Wang and Y. F. Zhang, *Mater. Sci. Eng*., C, 95 (2019) 78.
2. R. Manjunatha, D. H. Nagaraju, G. S. Suresh, J. S. M. Souza, Stanislaus F. D' and T. V. Venkateshad, *Electrochim. Acta*, 56 (2011) 6619.
3. X. Y. Kong, Y. Y. Wang, Q. Q. Zhang, T. R. Zhang, Q. Q. Teng, L. Wang, H. Wang and Y. F. Zhang, *J. Colloid Interface Sci*., 505 (2017) 615.
4. A. Cernata, M. Tertis, R. S?andulescua, F. Bedioui, A. Cristea and C. Criste, *Anal. Chim. Acta*, 886 (2015) 16.
5. O. S. Fatoki, B. O. Opeolu, B. Genthe and O. S. Olatunji, *Heliyon*, 4 (2018) e01066.
6. H. Montaseri and P. B. C. Forbes, *Materialstoday*, 17 (2018) 480.
7. D. Easwaramoorthy, Y. C. Yu and H. J. Huang, *Anal. Chim. Acta*, 439 (2001) 95.
8. T. P. Ruiz, C. M. Lozano, V. Tomás, R. Galera and P. J., *Biomed. Anal*., 38 (2005) 87.
9. E. M. Mximnano, F. D. Lima, C. A. L. Cardoso and G. J. Arruda*, Electrochim. Acta*, 259 (2018) 66.
10. Z. F. Wang, G. Z. Gou, L. Shi, J. Yang, C. Xu, L. Zhang, A. P. Fan and Y. Min, *J. Appl. Polym. Sci*., (2018) 46720.
11. S. J. Guo, D. Wen, Y. M. Zhai, S. J. Dong and E. K. Wang, *ACS Nano*, 4 (2010) 3959.
12. S. J. Guo, S. J. Dong and E. K. Wang, *ACS Nano*, 4 (2010) 547.
13. Q. Wu, Y. X. Xu, Z. Y. Yao, A. R. Liu and G. Q. Shi, *ACS Nano*, 4 (2010) 1963.
14. D. Luo, X. Q. Zhang and H. S. Chen, *Int. J. Hydrogen Energy*, 44 (2019) 31192.
15. J. Ryu, S. H. Ku, H. Lee and C. B. Park, *Adv. Funct. Mater*, 20 (2010) 2132.
16. F. F. Ren, C. Y. Zhai, M. S. Zhu, C. Q. Wang, H. W. Wang, D. Bin, J. Guo, P. Yang and Y. K. Du, *Electrochim. Acta*, 153 (2015) 175.
17. W. Xie, C. Herrmann, K. Ko ¨mpe, M. Haase and S. Schu ¨lcker, *J. Am. Chem. Soc*., 133 (2011) 19302.
18. J. M. Yan, X. B. Zhang, T. Akita, M. Haruta and Q. Xu, *J. Am. Chem. Soc*., 132 (2010) 5326.
19. P. Gnanaprakasam, J. S. E and T. Selvaraju, *J. Mater. Chem*. A, 3 (2015) 18010.
20. G. H. Yang, Y. J. Li, R. K. Ranab and J. J. Zhu, *J. Mater. Chem*. A, 1 (2013) 1754.
21. Y. Shi, T. T. Zhai, Y. Zhou, W. X. Xu, D. R. Yang, F. B. Wang and X. H. Xia, *J. Electroanal. Chem*., 819 (2018) 442.
22. G. FRENS, *Nature Physical science*, 241 (1973) 20.
23. W. S. Hummers and R. E. Offeman, *J. Am. Chem. Soc*., 80 (1958) 1339.
24. J. L. Wang, F. J. Trindade, C. B. d. Aquino, J. C. Pieretti, S. H. Domingues, R. A. Ando and P. H. C. Camargo, *Chem. Eur. J.,* 21 (2015) 9889.
25. J. Manna, S. Akbayrak and S. Özkar, *Applied Catalysis B: Environmental*, 208 (2017) 104.
26. J. D. Qiu, L. Shi, R. P. Liang, G. C. Wang and X. H. Xia, *Chem. Eur. J*, 18 (2012) 7950.
27. S. Su, C. Zhang, L. H. Yuwen, X. F. Liu, L. H. Wang, C. H. Fan and L. H. Wang, *Nanoscale*, 8 (2016) 602.
28. A. A. Vernekar and G. Mugesh, *Chem. Eur. J*., 18 (2012) 15122.
29. Y. Si and E. T. Samulski, *Nano Lett.*, 8 (2008) 1679.
30. R. J. Liu, S. W. Li, X. L. Yu, G. J. Zhang, S. J. Zhang, J. N. Yao, B. Keita, L. Nadjo and L. J. Zhi, *Small,* 8 (2012) 1398.
31. B. Y. Xia, W. T. Ng, H. B. Wu, X. Wang and X. W. Lou, *Angew. Chem., Int. Ed.,* 51 (2012) 7213.
32. X. Zhang, K. P. Wang, L. N. Zhang, Y. C. Zhang and L. Shen, *Anal. Chim. Acta*, 1036 (2018) 26.
33. D. B. Lu, Y. Zhang, L. T. Wang, S. X. Lin, C. M. Wang and X. F. Chen, *Talanta*, 88 (2012) 181.
34. K. Sheng, L. Wang, H. C. Li, L. Zou and B. X. Ye, *Talanta*, 164 (2017) 249.
35. E. Laviron, *J. Electroanal. Chem*., 52 (1974) 355.
36. J. L. Wang, J. e. Huo, J. Li, E. Shangguan and Q. M. Li, *Anal. Methods*, 5 (2013) 4119.

37. S. M. Yu, H. F. Li, G. G. Li, L. T. Niu, W. L. Liu and X. Di, *Talanta*, 184 (2018) 244.
38. M.E. Ghica, G.M. Ferreira and C.M.A. Brett, *J. Solid State Electrochem*., 19 (2015) 2869.
39. L. Fu, G. S. Lai and A. M. Yu, *RSC Adv*., 5 (2015) 76973.
40. M. M. Barsan, C. T. Toledo and C. M. A. Brett, *J. Electroanal. Chem*., 736 (2015) 8.
41. W. M. Si, W. Lei, Z. Han, Y. H. Zhang, Q. L. Hao and M. Z. Xia, *Sensors Actuators B: Chem*., 193 (2014) 823